J. Marine Sci. Appl. (2017) 16
DOI: https://doi.org/10.1007/s11804-017-1430-x

Numerical Simulation of the Solitary Wave Interacting with an Elastic Structure Using MPS-FEM Coupled Method

Chengping Rao, Youlin Zhang and Decheng Wan*

State Key Laboratory of Ocean Engineering, School of Naval Architecture, Ocean and Civil Engineering, Shanghai Jiao Tong University, Collaborative Innovation Center for Advanced Ship and Deep-Sea Exploration, Shanghai 200240, China

Abstract: Fluid-Structure Interaction (FSI) caused by fluid impacting onto a flexible structure commonly occurs in naval architecture and ocean engineering. Research on the problem of wave-structure interaction is important to ensure the safety of offshore structures. This paper presents the Moving Particle Semi-implicit and Finite Element Coupled Method (MPS-FEM) to simulate FSI problems. The Moving Particle Semi-implicit (MPS) method is used to calculate the fluid domain, while the Finite Element Method (FEM) is used to address the structure domain. The scheme for the coupling of MPS and FEM is introduced first. Then, numerical validation and convergent study are performed to verify the accuracy of the solver for solitary wave generation and FSI problems. The interaction between the solitary wave and an elastic structure is investigated by using the MPS-FEM coupled method.

Keywords: mesh-free method, moving particle semi-implicit, finite element method, fluid-structure interaction, solitary wave, MLParticle-SJTU solver

1 Introduction

The solitary wave is a type of peculiar wave with its profile located above the surface. It is typically used to simulate the tsunami wave, storm-induced wave, or other extreme sea conditions. The solitary wave impacting onto a structure usually leads to the deformation of or even damage to offshore structures such as floating production storage and offloading and liquefied natural gas carriers (Sriram and Ma, 2012). The interaction between the solitary wave and a structure needs to be investigated to prevent the operation of facilities from being affected. However, conducting numerical research on the interaction between the solitary wave and an elastic structure is difficult due to challenges in predicting the instantaneous impact load of the solitary wave and the deformation of the structure. In this paper, we will address the challenging FSI problem by using numerical approaches.

Many numerical methods have been developed to solve the Fluid-Structure Interaction (FSI) problems. The coupling strategies for FSI problems are primarily classified into partitioned (or weak) and monolithic (or strong) approaches. In the monolithic approach, a single system of equations that consider both fluid and structure domains is established. The main advantage of the monolithic approach is the stability of the solution process. However, the equation is difficult to form without any modifications for complex engineering problems and much more expensive to solve (Longatte *et al*., 2009). Particle Finite Element Method (PFEM) (Idelsohn, 2008) and space-time FEM (Walhorn *et al*., 2005; Aliabadi and Tezduyar, 1993) are two typical FSI computational methods based on the monolithic approach. By contrast, the partitioned approach divides the computational field into fluid and structure parts, the governing equations of which are solved separately. Interfacial conditions are imposed explicitly by exchanging the information between fluid and structure solutions. Given the modularity of the partitioned approach, it takes advantage of the already mature computation codes for fluid or structure analysis, which have been validated by solving complicated problems. The main challenge for the partitioned approach is to coordinate disciplinary algorithms to ensure the accuracy and efficiency of the FSI solution (Hou, 2012).

Currently, most numerical analyses for FSI problems are based on the grid system. Further effort is needed for FSI analysis when using mesh-based methods such as finite volume method and finite difference method, which involve tracing the surface of the fluid (Hirt and Nichols, 1981; Stanley and Fedkiw, 2003), information exchange between the structure and fluid domains, and updating the distorted meshes. Various mesh-morphing algorithms for FSI analysis are proposed to address these problems (el Moctar *et al*., 2017). The difficulties brought about by mesh can be eliminated when a Lagrangian description method is adopted.

Among the Lagrangian description methods, the Smoothed Particle Hydrodynamics (SPH) method (Lucy, 1977) and Moving Particle Semi-implicit (MPS) method

Received date: 09-Dec-2016
Accepted date: 28-Jul-2017
Foundation item: Supported by the National Natural Science Foundation of China (51379125, 51490675, 11432009, 51579145), pthe Chang Jiang Scholars Program (T2014099), the Shanghai Excellent Academic Leaders Program (17XD1402300), the Program for Professor of Special Appointment (Eastern Scholar) at Shanghai Institutions of Higher Learning (2013022), the Innovative Special Project of the Numerical Tank of the Ministry of Industry and Information Technology of China (2016-23/09), and Lloyd's Register Foundation for doctoral students
***Corresponding author Email:** dcwan@sjtu.edu.cn

(Koshizuka, 1996) are two representative particle-based methods for hydrodynamics in which the computational field is discretized as numerous moving particles. These methods can be especially effective while studying problems characterized by large displacements of the fluid-structure interface and rapidly moving fluid surface. In this type of problem, the fluid-structure interface and flow surface can be easily obtained without any specific treatments by the particle-based method. The MPS method uses a Lagrangian description to model fluid particles whose movement is computed from the interaction forces between particles (Chen *et al*., 2007). This approach removes difficulties in the treatment of the convective terms. Furthermore, mesh is not needed since MPS is a particle-based method. Numerous studies have been conducted on wave-structure interaction problems based on particle methods. For example, Altomare *et al*. (2015) employed the SPH method to study the wave-induced force on coastal structures and obtained reliable results through comparisons of experimental and semi-empirical results. Liang *et al*. (2017) investigated the solitary wave interaction with a movable seawall on the basis of incompressible SPH. Zhang and Wan (2017) simulated the interaction between waves and a free-rolling body using MPS method. The obtained Response Amplitude Operators (RAO) for roll motions are in agreement with experimental data.

The main objective of this study is to apply the MPS-FEM coupled method to investigate the interaction between the solitary wave and an elastic structure. The MPS method is used to calculate the fluid domain, whereas the FEM method is adopted for the structure domain. The coupled method combines the advantages of the individual methods and can thus achieve efficient and robust results. These two methods are coupled in a partitioned approach. This paper is organized as follows: The numerical schemes of MPS and FEM are introduced first, and the coupling strategy for the two methods is presented. Subsequently, a benchmark case of dam-break flow interacting with an elastic gate is studied to verify the capability of the proposed solver in solving FSI problems. Then, a convergence study for the wave-structure interaction problem is conducted to find the appropriate particle spacing. Finally, the proposed MPS-FEM coupled method is applied to the simulation of the solitary wave interacting with an elastic structure.

2 Numerical methods

In this paper, the fluid domain is calculated by our in-house particle solver MLParticle-SJTU on the basis of the improved MPS method. The original MPS method suffers from many problems, such as pressure oscillation, energy non- conservation, computational instability, and low precision. To address these problems, a number of enhancements were proposed (Khayyer *et al*., 2008; Kondo and Koshizuka, 2011; Khayyer and Gotoh, 2013). The improvements for the original MPS employed in the proposed solver were elaborated in our previous papers (Zhang and Wan, 2011; Zhang *et al*., 2014; Tang and Wan, 2015). The solver has been proven to be valid in the simulation of surface flow (Tang *et al*., 2016a, 2016b), such as dam-break, sloshing, water-entry, and wave-body interaction (Zhang *et al*., 2016). In this section, the mathematical equations of MPS and FEM, together with numerical solitary wave generation, are introduced. The coupling strategy for MPS and FEM is then described.

2.1 Fluid solver based on MPS

The governing equations for viscous incompressible fluid contain continuity equation and a Navier–Stokes equation:

$$\nabla \cdot \boldsymbol{V} = 0 \tag{1}$$

$$\frac{\mathrm{D}\boldsymbol{V}}{\mathrm{D}t} = -\frac{1}{\rho}\nabla P + \nu \nabla^2 \boldsymbol{V} + \boldsymbol{g} \tag{2}$$

where ρ is the fluid density, P is the pressure, $\boldsymbol{V}$ is the velocity vector, $\boldsymbol{g}$ is the gravitational acceleration, and v is the kinematic viscosity. In the particle method, governing equations are transformed to equations of the particle interactions. The particle interaction models are based on the kernel function. This paper adopts a modified kernel function (Zhang and Wan, 2012).

$$W(r) = \begin{cases} \dfrac{r_e}{0.85r + 0.15r_e} - 1 & 0 \le r < r_e \\ 0 & r_e \le r \end{cases} \tag{3}$$

where $r = |\boldsymbol{r}_j - \boldsymbol{r}_i|$ is the distance between particle i and j, and r_e is the radius of effect.

In the MPS method, the models of particle interaction involve the gradient, divergence, and Laplacian models. They are written as

$$\langle \nabla \phi \rangle_i = \frac{D}{n^0} \sum_{j \ne i} \frac{\phi_j + \phi_i}{|\boldsymbol{r}_j - \boldsymbol{r}_i|^2} (\boldsymbol{r}_j - \boldsymbol{r}_i) \cdot W(|\boldsymbol{r}_j - \boldsymbol{r}_i|) \tag{4}$$

$$\langle \nabla \cdot \boldsymbol{V} \rangle_i = \frac{D}{n^0} \sum_{j \ne i} \frac{(\boldsymbol{V}_j - \boldsymbol{V}_i) \cdot (\boldsymbol{r}_j - \boldsymbol{r}_i)}{|\boldsymbol{r}_j - \boldsymbol{r}_i|^2} W(|\boldsymbol{r}_j - \boldsymbol{r}_i|) \tag{5}$$

$$\langle \nabla^2 \phi \rangle_i = \frac{2D}{n^0 \lambda} \sum_{j \ne i} (\phi_j - \phi_i) \cdot W(|\boldsymbol{r}_j - \boldsymbol{r}_i|) \tag{6}$$

$$\lambda = \frac{\sum_{j \ne i} W(|\boldsymbol{r}_j - \boldsymbol{r}_i|) |\boldsymbol{r}_j - \boldsymbol{r}_i|^2}{\sum_{j \ne i} W(|\boldsymbol{r}_j - \boldsymbol{r}_i|)} \tag{7}$$

where D is the dimension number, $\boldsymbol{r}$ is the position vector, and n^0 is the initial density of the particle number and defined as

$$\langle n \rangle_i = \sum_{j \ne i} W(|\boldsymbol{r}_j - \boldsymbol{r}_i|) \tag{8}$$

As noted previously, the MPS method is used to simulate the incompressible flow. To ensure the incompressibility of the fluid, a semi-implicit algorithm is adopted, and pressure fields are obtained by solving the pressure Poisson equation. In this work, we employ a mixed source term method combined with a velocity divergence-free condition and a

constant particle number density, as proposed by Tanaka (Tanaka and Masunaga, 2010) and rewritten as (Lee *et al*., 2011)

$$\left\langle \nabla^2 P^{k+1} \right\rangle_i = (1-\gamma)\frac{\rho}{\Delta t}\nabla \cdot V_i^* - \gamma \frac{\rho}{\Delta t^2}\frac{< n^k >_i - n^0}{n^0} \tag{9}$$

where Δt is the calculation time step, k and k+1 indicate the physical quantity in the kth and (k+1)th time steps, and γ is the weight of the particle number density term in the right-hand side of Eq. (9) and is assigned a value between 0 and 1. In this paper, γ =0.01 is selected for all numerical experiments.

2.2 Structure solver based on FEM

According to FEM theory, the spatially discretized structural dynamic equations, which govern the motion of structural nodes, can be expressed as (Iura and Atluri, 1995)

$$\boldsymbol{M}\ddot{\boldsymbol{y}} + \boldsymbol{C}\dot{\boldsymbol{y}} + \boldsymbol{K}\boldsymbol{y} = \boldsymbol{F}(t) \tag{10}$$

$$\boldsymbol{C} = \alpha_1 \boldsymbol{M} + \alpha_2 \boldsymbol{K} \tag{11}$$

where $\boldsymbol{M}$, $\boldsymbol{C}$, $\boldsymbol{K}$ are the mass matrix, the Rayleigh damping matrix, and the stiffness matrix of the structure, respectively. $\boldsymbol{F}$ is the external force vector that acts on the structure and varies with computational time. $\boldsymbol{y}$ is the displacement vector of the structure. α_1 and α_2 are coefficients related with the natural frequency and the damping ratios of the structure.

According to Newmark (1959), the structural nodal displacement at t=t+Δt can be solved with the help of Taylor's expansions of velocity and displacement

$$\dot{\boldsymbol{y}}_{t+\Delta t} = \dot{\boldsymbol{y}}_t + (1-\gamma)\ddot{\boldsymbol{y}}_t \Delta t + \gamma \ddot{\boldsymbol{y}}_{t+\Delta t}\Delta t,\ 0<\gamma<1 \tag{12}$$

$$\boldsymbol{y}_{t+\Delta t} = \boldsymbol{y}_t + \dot{\boldsymbol{y}}_t \Delta t + \frac{1-2\beta}{2}\ddot{\boldsymbol{y}}_t \Delta t^2 + \beta \ddot{\boldsymbol{y}}_{t+\Delta t}\Delta t^2,\ 0<\beta<1 \tag{13}$$

where β and γ are important parameters of the Newmark method and are selected as β=0.25, γ=0.5 for all simulations in this paper. From Eqs. (12) and (13), we can obtain the expressions of $\ddot{y}_{t+\Delta t}$ and $\dot{y}_{t+\Delta t}$ in the form of $y_{t+\Delta t}$, $\dot{y}_t$, and y_t (Hsiao *et al*., 1999)

$$\ddot{\boldsymbol{y}}_{t+\Delta t} = a_0(\boldsymbol{y}_{t+\Delta t} - \boldsymbol{y}_t) - a_2\dot{\boldsymbol{y}}_t - a_3\ddot{\boldsymbol{y}}_t \tag{14}$$

$$\dot{\boldsymbol{y}}_{t+\Delta t} = \dot{\boldsymbol{y}}_t + a_6\ddot{\boldsymbol{y}}_t + a_7\ddot{\boldsymbol{y}}_{t+\Delta t} \tag{15}$$

$$\begin{aligned} &a_0 = \frac{1}{\beta\Delta t^2},\ a_1 = \frac{\gamma}{\beta\Delta t},\ a_2 = \frac{1}{\beta\Delta t},\ a_3 = \frac{1}{2\beta} - 1, \\ &a_4 = \frac{\gamma}{\beta} - 1, a_5 = \frac{\Delta t}{2}\left(\frac{\gamma}{\beta} - 2\right),\ a_6 = \Delta t(1-\gamma),\ a_7 = \gamma\Delta t \end{aligned} \tag{16}$$

where $a_0 \sim a_7$ are the parameters related to β, γ, and Δt. After combined with Eq. (14) and (15), Eq. (10) can be transformed into Eq. (17) as below

$$\bar{\boldsymbol{K}}\,\boldsymbol{y}_{t+\Delta t} = \bar{\boldsymbol{F}}_{t+\Delta t} \tag{17}$$

$$\bar{\boldsymbol{K}} = \boldsymbol{K} + a_0\boldsymbol{M} + a_1\boldsymbol{C} \tag{18}$$

$$\bar{\boldsymbol{F}}_{t+\Delta t} = \boldsymbol{F}_t + \boldsymbol{M}(a_0\boldsymbol{y}_t + a_2\dot{\boldsymbol{y}}_t + a_3\ddot{\boldsymbol{y}}_t) + \boldsymbol{C}(a_1\boldsymbol{y}_t + a_4\dot{\boldsymbol{y}}_t + a_5\ddot{\boldsymbol{y}}_t) \tag{19}$$

$\bar{\boldsymbol{K}}$ and $\bar{\boldsymbol{F}}$ are the so-called effective stiffness matrix and effective force vector in the constructed Eq. (17), respectively. Then, the displacement $y_{t+\Delta t}$ that corresponds to the next time step can be obtained by solving Eq. (17). Finally, the accelerations and velocities at the next time step are updated by using Eqs. (14) and (15). The $y_{t+\Delta t}$, $\dot{y}_{t+\Delta t}$ and $\ddot{y}_{t+\Delta t}$ are herein updated from y_t, $\dot{y}_t$, and $\ddot{y}_t$.

2.3 Coupling strategy for MPS-FEM coupled method

In this study, the partitioned coupling between MPS and the FEM method is implemented. The time step sizes for structure and fluid analyses are Δt_s and Δt_f, respectively. Here Δt_s is k multiples of Δt_f, where k is an integer. k is set to 1, which indicates that the time steps for the structure and fluid analyses are the same. The interaction procedure can be summarized as follows:

1) The fluid field is calculated k times based on the MPS method. The pressure of the fluid wall boundary particle is calculated as follows:

$$\bar{p}_{n+1} = \frac{1}{k}\sum_{i=1}^{k} p_{n+i} \tag{20}$$

where p_{n+i} is the pressure of the fluid particle on the wall boundary at the instant $t + i\Delta t_f$, and $\bar{p}_{n+1}$ is the average pressure of the fluid particle within Δt_s.

2) The values of structural nodal position y_t, velocity $\dot{y}_t$, and acceleration $\ddot{y}_t$ are determined based on the results at the previous time step.

3) The external force vector $\boldsymbol{F}_{t+\Delta t_s}$ of the structural boundary particles is calculated by multiplying the average pressure $\bar{p}_{n+1}$ and the influential area, which equals the square of the initial particle spacing dp.

$$\boldsymbol{F}_{t+\Delta t_s} = \bar{p}_{n+1} \cdot dp^2 \tag{21}$$

4) The new values of structural nodal displacements and velocities are calculated based on the Newmark method described in the previous section.

5) The velocity and position of the structural boundary particles and fluid particles are updated.

2.4 Numerical generation of solitary wave

In theory, a solitary wave consists of a single crest of infinite length. According to potential flow theory, the profile of the solitary wave can be expressed as follows (Boussinesq, 1872; Korteweg and De Vries, 1895):

$$\eta = H\mathrm{sech}^2(k(x-ct)) \tag{22}$$

$$k = \sqrt{3H/4d^3} \tag{23}$$

$$c = \sqrt{g(H+d)} \tag{24}$$

where H is the wave height, d is the water depth, x is the horizontal coordinate, c is the wave speed, g is the acceleration of gravity, and t is the time.

In this paper, the solitary wave is generated by a piston-type wavemaker; its motion was described by Goring

(1978). The speed of the wavemaker is

$$U(t)=\frac{\mathrm{d}X(t)}{\mathrm{d}t}=\frac{cH\mathrm{sech}^2(k(X-ct))}{d+H\mathrm{sech}^2(k(X-ct))} \tag{25}$$

Thus, the position of the wavemaker at time t can be expressed as

$$X(t)=\frac{H}{kd}\tanh(k(ct-X)) \tag{26}$$

The stroke length is calculated by the difference value between the wavemaker position at $t=+\infty$ and $t=-\infty$

$$S=\sqrt{\frac{16Hd}{3}} \tag{27}$$

The wave period is approximately

$$T\approx\frac{2}{kc}(3.8+\frac{H}{d}) \tag{28}$$

After one wave period, the wavemaker reaches its maximum position and then becomes still.

3 Numerical validations

To check the convergence and accuracy of the calculated results, a benchmark case (Antoci *et al*., 2007) of a dam-break flow interacting with an elastic gate is investigated in this section. As shown in Fig. 1, a two-dimensional tank is filled by a water column with the depth of 0.14 m and width of 0.1 m. An elastic gate is installed at the lower part of the left wall of the tank. The upper end of the gate is consolidated, while the lower end is free to deform.

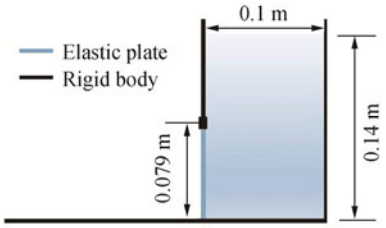

Fig. 1 Schematic view of a dam-break with elastic gate

3.1 Convergence study

To investigate the effects of particle spacing and element length on the numerical results, the convergence study is conducted. The calculation parameters are shown in Table 1. According to Euler–Bernoulli beam theory, the natural frequency of the elastic gate is calculated to be 8.27 Hz. The damping coefficients α_1 and α_2 are set to 0 and 0.025 in this case, respectively.

For the proposed MPS-FEM coupled method, the element nodes overlap the ghost particles in the boundary, thereby indicating that the element length for structure analysis equals the particle spacing for fluid analysis. Three different spatial resolutions (0.000 5, 0.001, 0.002 m), whose configurations are listed in Table 2, are employed to check the convergence of the numerical results. The calculation time step is set based on the Courant–Friedrichs–Lewy (CFL) stability condition.

$$\Delta t\le\frac{C_{\max}\cdot dp}{u_{\max}} \tag{29}$$

where Δt is the time step, $u_{\max}$ is the maximum instantaneous velocity of particles, dp is the initial particle spacing, and $C_{\max}$ is the upper bound of the Courant number, which is set to 0.1 in this study.

A comparison of the displacement history on the endpoint of elastic gate with different spatial resolutions is shown in Fig. 2. A similar tendency can be observed that the displacements in both horizontal and vertical directions reach the maximum at 0.167 s and then decrease slowly after the peak. The displacement histories of the fine (Case 1) and medium-resolution (Case 2) cases show good agreement, whereas the coarse-resolution case (Case 3) shows an evident discrepancy. The peak values of the displacement history are listed in Table 3 to present the convergence of the simulations quantitatively. Table 3 shows that the maximum displacements stabilized despite a minimal relative difference. Thus, the obtained result in this section is convergent with respect to the spatial resolution.

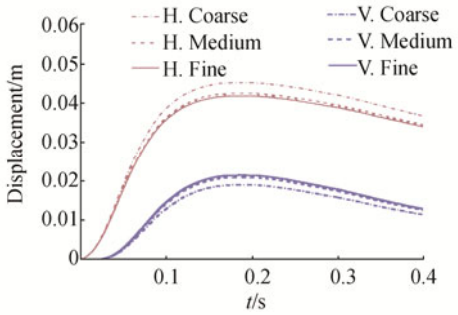

Fig. 2 Displacement history on the endpoint of the gate

3.2 Results and discussion

To validate the accuracy of the proposed solver, numerical results of the benchmark case are compared with experimental results at the same instants with an interval of 0.08 s. Snapshots of the deformation of the elastic gate and elevation of the free surface are shown in Fig. 3. The elastic gate starts to bend because of hydrostatic pressure. Then, a clearance exists between the gate and bottom through which the fluid could flow. The displacement at the endpoint of the gate continues to increase and reaches its maximum. An evident decrease in flow velocity could be observed after 0.2 s. In addition, the profiles of the deformed baffle and the free surface coincide with those of the experimental results (Antoci *et al*., 2007).

Time histories of horizontal and vertical displacements at the endpoint of the gate are shown in Fig. 4. The horizontal displacement agrees well with the experimental result, whereas the numerical simulation overestimates the vertical displacement slightly (6%) around the maximum. The comparison between the numerical results and the experiment data shows that the displacement of gate is well reproduced by the proposed MPS-FEM coupled method. This finding indicates that the proposed solver can solve FSI

problems with free surface.

4 Numerical simulations for solitary wave-structure interaction

Wave-structure interaction is numerically investigated in this section. The solitary wave is generated by a piston-type wavemaker in a numerical wave flume. Fig. 5 shows the geometric setup of the numerical wave flume, which is the same as that presented by Betsy (2014). The wave height (amplitude) of the solitary wave is set to 0.034 3 m, and the water depth is 0.114 m. The interactions between the solitary wave with a rigid plate and that with a flexible plate are simulated. The effects of the structure's flexibility on flow are primarily investigated.

4.1 Numerical conditions and convergence study

A convergence study is performed to explore the convergence of the FSI simulation with respect to the spatial resolution. Three different spatial resolutions (0.004, 0.002, and 0.001 m), whose configurations are listed in Table 4, are considered in the simulations. The computational parameters in the simulations are shown in the fluid part of Table 5. The wave-elevation gauge H1 is set at a distance of 0.61 m from the piston.

Numerical pressure contours (Case 2) at different instants are shown in Fig. 6, from which the propagation of the solitary wave can be observed. The solitary wave forms at 1.5 s and reaches the right end of the fume at 3.5 s. Then, the wave reflects back to the upstream soon after impacting on the wall. The pressure field is fairly smooth, and no evident decay for the wave height is observed during propagation.

Fig. 7 shows a comparison of the wave-elevation history at H1 point with different spatial resolutions and the experimental result. The convergent result can be obtained for Cases 2 and 3. However, the maximum wave elevation for Case 1 is evidently higher (7.3%) than the desired value. Moreover, the steepness of the curve for the coarse-resolution case after the peak is relatively smaller than the other two cases. The differences between the result of the medium and fine-resolution cases are almost negligible. Furthermore, the numerical wave elevation (medium, dp = 0.002 m) and the experiment result (Betsy, 2014) show good agreement, thereby indicating that a particle spacing of 0.002 m can achieve the desired solitary wave.

Then, the interaction between solitary wave and a flexible plate is investigated by using the in-house solver with the expansion of the MLParticle-SJTU solver based on the MPS-FEM coupled method. The geometric setup and the computational parameters (Cases 4–6) are the same as in previous cases (Cases 1–3). However, the wall on the right end of the flume is replaced by a simply supported elastic structure with a consolidated bottom. The computational parameters for the fluid and structure calculations are shown in Table 5. The natural frequency of the elastic structure is 11.3 Hz according to the Euler–Bernoulli beam theory. The element type employed in the structural calculation is a two-node planar beam element. The displacement of the structure in the middle point is recorded during the calculation. Four pressure gauges (P1, P2, P3, and P4) are set on the structure to record the pressure history. Their vertical distances from the bottom are 0.140, 0.120, 0.114, and 0.09 m, respectively.

To verify the convergence of the simulations, the results with different particle spacings are compared in Figs. 8 and 9. The displacement history (on the middle point) and pressure history (on P4 point) show good agreement. Their peak values and the relative errors with respect to the fine spatial resolution (Case 6) are listed in Table 6. For the medium spatial resolution (Case 5), the relative errors for the maximum pressure and displacement are 2.5% and 1.7% respectively, which indicates that the FSI simulation results are convergent.

The hardware that was used for the simulations includes an Intel Core i7-4790 processor @ 3.60 GHz with 8 threads and 16 GB of memory. The time consumed on each case is shown in Fig. 10. The consumed time increases dramatically with the refinement of the particle and the element.

Table 1 Parameters for computation

Item	Parameters	Value
Structure	Cross area/m^2	0.005
	Elastic modulus/MPa	10.0
	Damping coefficient α_1	0
	Damping coefficient α_2	0.025
Fluid	Water density/($kg \cdot m^{-3}$)	1 000
	Kinematic viscosity/($m^2 \cdot s^{-1}$)	1×10^{-6}
	Gravitational acceleration/($m \cdot s^{-2}$)	9.81

Table 2 Configurations for cases

Case No.	Particle spacing/m	Particle number	Element length/m	Element number	Time step/s
1	0.000 5	55 720	0.000 5	158	0.000 02
2	0.001	13 860	0.001	78	0.000 05
3	0.002	3 430	0.002	39	0.000 1

Table 3 Peak value in the displacement history

Case No.	Disp. in Hor./m	Relative difference/%	Disp. in Ver./m	Relative difference/%
1	0.041 77	-	0.021 41	-
2	0.042 45	1.6	0.020 84	−2.6
3	0.045 16	8.1	0.018 94	−11.5

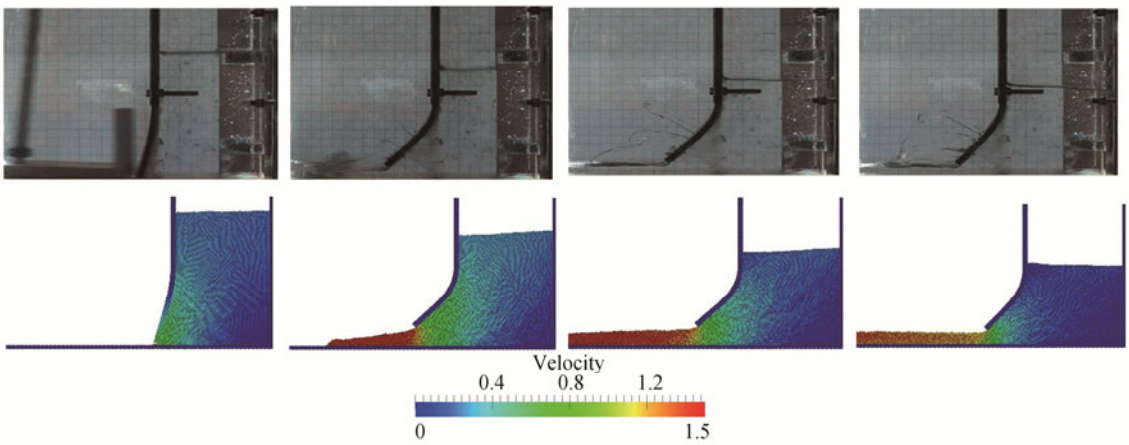

(a) t=0.04 s (b) t=0.12 s (c) t=0.20 s (d) t=0.28 s

Fig. 3 Snapshots of deformation and free surface (top: experiment from Antoci *et al.* (2007); bottom: present result in Case 2)

Table 4 Configurations for cases

Cases	Plate condition	Particle spacing/m	Particle number	Element length/m	Element number	Time step/s
1	Rigid	0.004	17 472	-	-	0.000 2
2	Rigid	0.002	71 193	-	-	0.000 1
3	Rigid	0.001	284 886	-	-	0.000 05
4	Elastic	0.004	17 472	0.004	55	0.000 2
5	Elastic	0.002	71 193	0.002	110	0.000 1
6	Elastic	0.001	284 886	0.001	220	0.000 05

Table 5 Parameters for computation

Item	Parameters	Value
Structure	Cross area/m^2	0.004
	Elastic modulus/MPa	50.0
	Damping coefficient α_1	0
	Damping coefficient α_2	0.025
Fluid	Water density/($kg \cdot m^{-3}$)	1 000
	Kinematic viscosity/($m^2 \cdot s^{-1}$)	1×10^{-6}
	Gravitational acceleration/($m \cdot s^{-2}$)	9.81

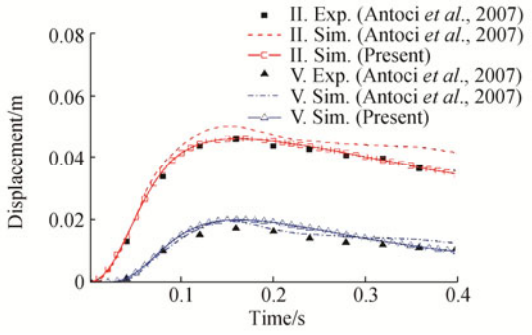

Fig. 4 Horizontal and vertical displacements of the free end of the gate

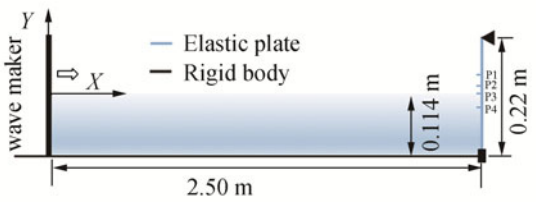

Fig. 5 Geometric setup of the numerical wave flume

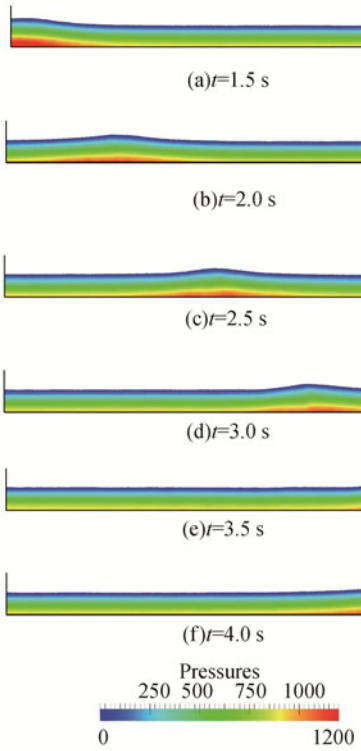

Fig. 6 Propagation of the solitary wave in the flume (Case 2)

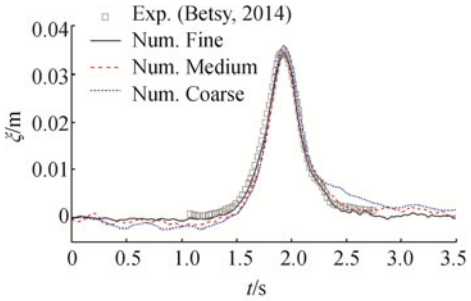

Fig. 7 Comparison of wave-elevation history at H1 (dot: Case 1; dash: Case 2; solid: Case 3; square: Betsy (2014))

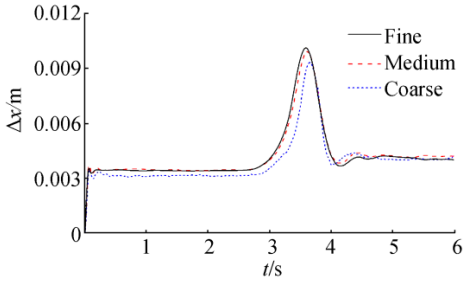

Fig. 8 Comparison of displacement history on the midpoint of the plate (dot: Case 4; dash: Case 5; solid: Case 6)

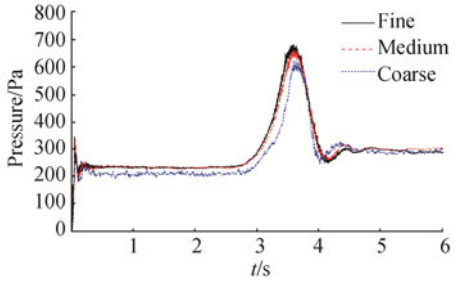

Fig. 9 Pressure history on P4 point (coarse: Case 4; medium: Case 5; fine: Case 6)

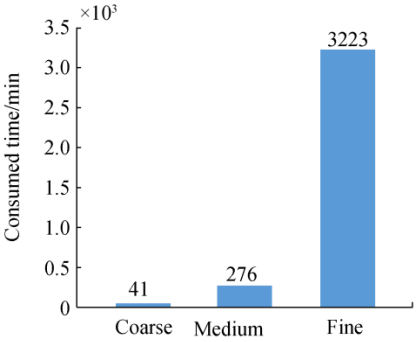

Fig. 10 Time consumed on the FSI simulations (coarse: Case 4; medium: Case 5; fine: Case 6)

Table 6 Comparison of results of the FSI simulations

Case No.	Max. Dis./m	Relative difference/%	Max. pres./Pa	Relative difference/%
4	0.009 75	5.7	623.3	6.6
5	0.010 16	1.7	650.9	2.5
6	0.010 34	-	667.4	-

4.2 Results and discussion

The results of the aforementioned numerical simulation (Case 5) are discussed in this subsection. The effects of the structural flexibility on the interaction are mainly investigated. As shown in Fig. 8, the structure slightly bends and stabilizes (Δx=0.003 5 m) quickly at the beginning because of the hydrostatic pressure acting onto the structure. Then, at 3 s, the structure begins to be impacted by the solitary wave, and the solitary wave propagates to the right end of the flume. At 3.6 s, the displacement on structure reaches the maximum (Δx=0.01 m) and drops to the previous level soon after the slight oscillation owing to the structure damping.

The pressure time history on the gauges is shown in Fig. 11. The figure also shows the corresponding results for a rigid structure with the same spatial resolution (Case 2). According to the pressure history on the P3 point, the duration of the wave impact is approximately 1 s, which indicates that slamming did not occur in the present simulation. The maximum pressure on the rigid structure

appears at 3.5 s and is much greater than that on the elastic structure. However, the maximum pressure appears at 3.6 s for the elastic structure. This slight time discrepancy could be due to the flexibility of the elastic structure. Moreover, the pressure oscillates for the rigid structure, whereas the pressure is steady for the elastic structure because the energy is partially absorbed by the elastic structure and the flow field is relatively stable.

Comparative snapshots are presented in Fig. 12 to show the structural deformation of the elastic structure. At t=3.0 s, the wave propagates near the right end of the flume, and the elastic structure begins to be affected. As the wave crest approaches the wall, the surrounding water surface elevates evidently, and the deformation of the structure increases accordingly. Then, at t=3.6 s, the wave crest reaches the wall and impacts onto the elastic structure. The surface rises rapidly, and the deformation of the structure reaches the maximum. For the elastic structure, the water level near the wall is slightly lower than that for the rigid structure because the deformation of the structure provides extra space for the water. The surface and deformation return to the previous level as the wave reflects upstream.

During the interaction, no wave breaking or curling occurs on the surface, thereby possibly resulting in air entrapment. Thus, the effects of air phase can be ignored in this study. According to the research of Khayyer and Gotoh (2015) based on the multi-phase flow model, the cushioning effects of the air trapped between the structure and the fluid would noticeably reduce the impact pressure.

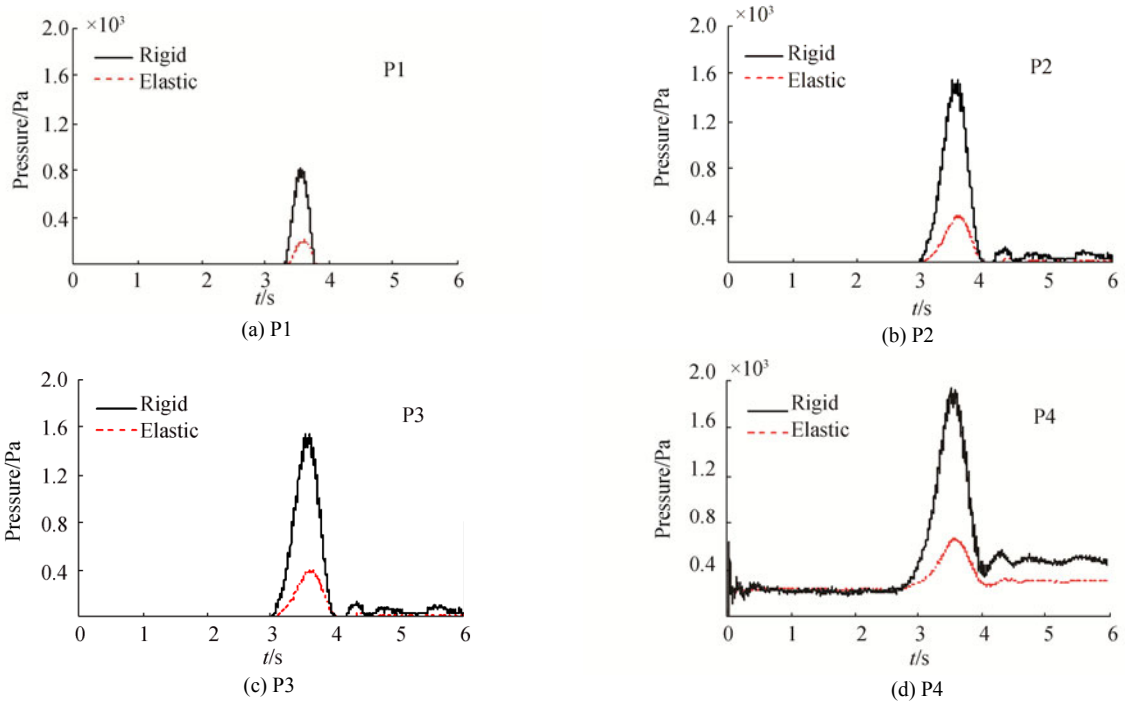

(a) P1 (b) P2 (c) P3 (d) P4

Fig. 11 Pressure history on P1–P4 (solid: Case 2; dash: Case 5)

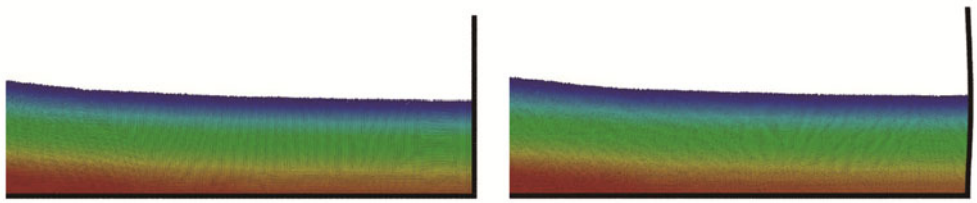

(a) t=3.0 s

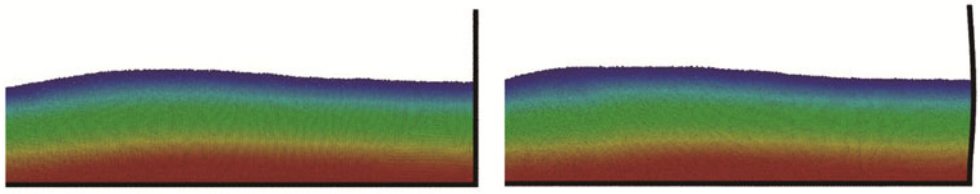

(b) t=3.3 s

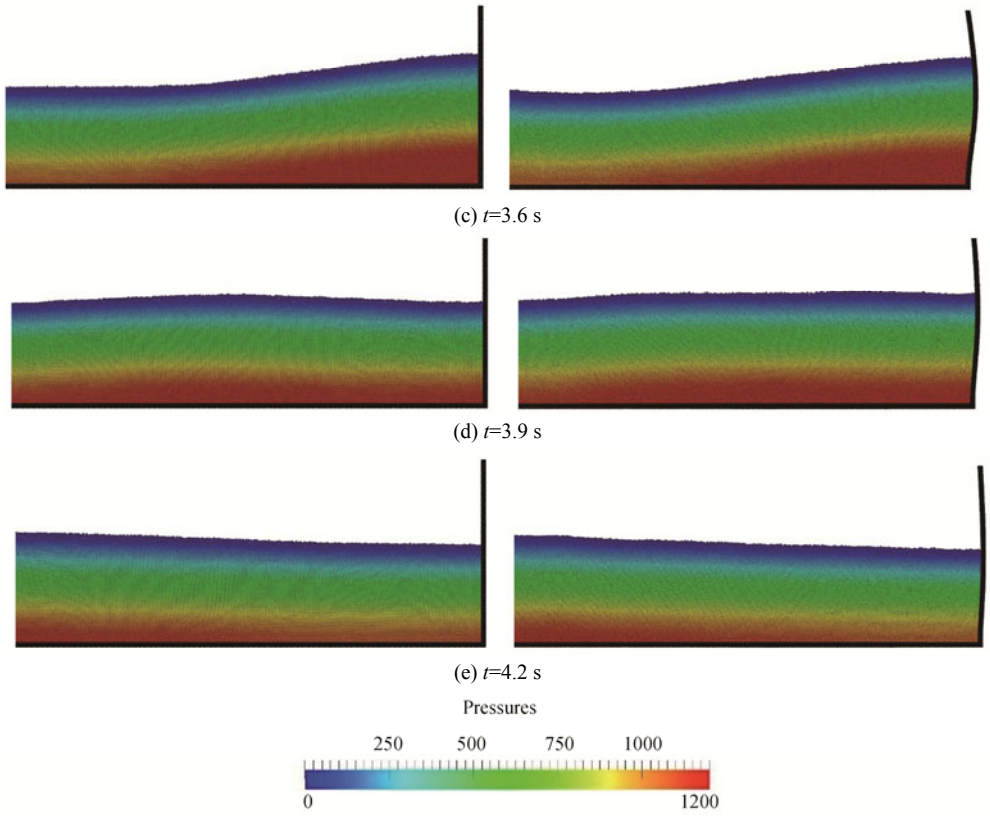

Fig. 12 Snapshots of structural deformation and flow field (left: Case 2; right: Case 5)

5 Conclusions

In this paper, the MPS-FEM coupled method is introduced to investigate the interaction between the solitary wave and an elastic structure. Theories of MPS and FEM, together with the coupled strategy, are introduced. In the numerical simulation, the benchmark case of dam-break flow interacting with an elastic gate is studied first. The time-dependent displacements of the free end of the gate, together with the free surface, are in good agreement with experimental data. This finding indicates that the proposed MPS-FEM coupled method efficiently solves FSI problems with free surface.

Subsequently, the FSI problem of the solitary wave interacting with an elastic structure is studied by using the MPS-FEM coupled method. A convergent study with respect to particle spacing is conducted. Results show that a particle spacing of 0.002 m can generate the desired solitary wave. In addition, the displacement and pressure history in the FSI simulations with different spatial resolutions are compared qualitatively and quantitatively. Convergent results are observed.

Finally, the effects of structural flexibility on the wave-structure interaction are investigated. The maximum pressure occurs at 3.5 s for the rigid case and occurs 0.1 s later for the flexible case. The water level near the wall is slightly lower in the elastic structure than in the rigid structure because the deformation of the structure provides extra space for the water. By comparing the results of case with rigid and elastic structure, it can be seen that the pressure on the elastic structure is much lower than that on the rigid structure. In other words, the flexibility of the structure relieves the impacting load of the solitary wave. Thus, the MPS-FEM coupled method can be applied to FSI problems with waves.

References

Aliabadi SK, Tezduyar TE, 1993. Space-time finite element computation of compressible flows involving moving boundaries and interfaces. *Computer Methods in Applied Mechanics and Engineering*, **107**(1-2), 209-223.

Altomare C, Crespo AJ, Domínguez JM, Gómez-Gesteira M, Suzuki T, Verwaest T, 2015. Applicability of smoothed particle hydrodynamics for estimation of sea wave impact on coastal structures. *Coastal Engineering*, **96**, 1-12.
DOI: 10.1016/j.coastaleng.2014.11.001

Antoci C, Gallati M, Sibilla S, 2007. Numerical simulation of fluid-structure interaction by SPH. *Computers & Structures*, **85**(11-14), 879-890.
DOI: 10.1016/j.compstruc.2007.01.002

Betsy S, 2014. Experiments and computations of solitary-wave forces on a coastal-bridge deck. Part I: Flat Plate. *Coastal Engineering*, **88**,194-209.
DOI: 10.1016/j.coastaleng.2014.01.005

Boussinesq J, 1872. Théorie des ondes et des remous qui se propagent le long d'un canal rectangulaire horizontal, en communiquant au liquide contenu dans ce canal des vitesses sensiblement pareilles de la surface au fond. *Journal de Mathématiques Pures et Appliquées*, **17**, 55-108. (in French)

Chen JKL, Noguchi H, Koshizuka S, 2007. Fluid-shell structure interaction analysis by coupled particle and finite element method. *Computers & Structures*, **85**(11-14), 688-697.
DOI: 10.1016/j.compstruc.2007.01.019

el Moctar O, Ley J, Oberhagemann J, Schellin T, 2017. Nonlinear computational methods for hydroelastic effects of ships in extreme seas. *Ocean Engineering*, **130**, 659-673.
DOI: 10.1016/j.oceaneng.2016.11.037

Goring DG, 1978. *Tsunamis-the propagation of long waves onto a shelf*. PhD thesis, California Institute of Technology, Pasadena.

Hirt CW, Nichols BD, 1981. Volume of fluid (VOF) method for the dynamics of free boundaries. *Journal of Computational Physics*, **39**(1), 201-225.

Hou G, 2012. Numerical methods for fluid-structure interaction -a review. *Communications in Computational Physics*, **12**(2), 337-377.
DOI: 10.4208/cicp.291210.290411s

Hsiao KM, Lin JY, Lin WY, 1999. A consistent co-rotational finite element formulation for geometrically nonlinear dynamic analysis of 3-D beams. *Comput. Methods Appl. Mech. Engrg*, **169**, 1-18.
DOI: 10.1016/S0045-7825(98)00152-2

Idelsohn SR, 2008. Unified Lagrangian formulation for elastic solids and incompressible fluids: Application to fluid-structure interaction problems via the PFEM. *Comput. Methods Appl. Mech. Eng*., **197**, 1762-1776.
DOI: 10.1016/j.cma.2007.06.004

Iura M, Atluri SN, 1995. Dynamic analysis of planar flexible beams with finite rotations by using inertial and rotating frames. *Computers and Structures*, **55**(3), 453-462.
DOI: 10.1016/0045-7949(95)98871-M

Khayyer A, Gotoh H, 2013. Enhancement of performance and stability of MPS mesh-free particle method for multiphase flows characterized by high density ratios. *Journal of Computational Physics*, **242**, 211-233.
DOI: 10.1016/j.jcp.2013.02.002

Khayyer A, Gotoh H, 2015. A multi-phase compressible -incompressible particle method for water slamming. *Proceedings of the Twenty-fifth International Ocean and Polar Engineering Conference*, Kona, Hawaii, USA, 1235-1240.
DOI: 10.17736/ijope.2016.mk42

Khayyer A, Gotoh H, Shao SD, 2008. Corrected incompressible SPH method for accurate water-surface tracking in breaking waves. *Coastal Engineering*, **55**(3), 236-250.
DOI: 10.1016/j.coastaleng.2007.10.001

Kondo M, Koshizuka S, 2011. Improvement of stability in moving particle semi-implicit method. *International Journal for Numerical Methods in Fluids*, **65**(6), 638-654.
DOI: 10.1002/fld.2207

Korteweg DJ, De Vries G, 1895. On the change of form of long waves advancing in a rectangular canal, and on a new type of long stationary waves. *The London, Edinburgh, and Dublin Philosophical Magazine and Journal of Science*, **39**, 422-443.
DOI: 10.1080/14786449508620739

Koshizuka S, 1996. Moving-particle semi-implicit method for fragmentation of incompressible fluid. *Nuclear Science & Engineering the Journal of the American Nuclear Society*, **123**(3), 421-434.

Lee BH, Park JC, Kim MH, Hwang SC, 2011. Step-by-step improvement of MPS method in simulating violent free-surface motions and impact-loads. *Computer Methods in Applied Mechanics & Engineering*, **50**(24), 5921-5933.
DOI: 10.1016/j.cma.2010.12.001

Liang DF, Jian W, Shao S, Chen R, Yang K, 2017. Incompressible SPH simulation of solitary wave interaction with movable seawalls. *Journal of Fluids and Structures*, **69**, 72-88.
DOI: 10.1016/j.jfluidstructs.2016.11.015

Longatte E, Verremana V, Souli M, 2009. Time marching for simulation of fluid-structure interaction problems. *Journal of Fluids and Structures*, **25**, 95-111.
DOI: 10.1016/j.jfluidstructs.2008.03.009

Lucy LB, 1977. A numerical approach to the testing of the fission hypothesis. *The Astronomical Journal*, **82**, 1013-1024.

Newmark NM, 1959. A method of computation for structural dynamics. *Journal of the Engineering Mechanics Division*, **85**(3), 67-94.

Sriram V, Ma QW, 2012. Improved MLPG_R method for simulating 2D interaction between violent waves and elastic structures. *Journal of Computational Physics*, **231**(22), 7650-7670.
DOI: 10.1016/j.jcp.2012.07.003

Stanley O, Fedkiw R, 2003. *Level set methods and dynamic implicit surfaces*. Springer, New York, 17-21.
DOI: 10.1115/1.1760520

Tanaka M, Masunaga T, 2010. Stabilization and smoothing of pressure in mps method by quasi-compressibility. *Journal of Computational Physics*, **229**(11), 4279-4290.
DOI: 10.1016/j.jcp.2010.02.011

Tang ZY, Wan DC, 2015. Numerical simulation of impinging jet flows by modified MPS method. *Engineering Computations*, **32**(4), 1153-1171.
DOI: 10.1108/EC-01-2015-0002

Tang ZY, Zhang YL, Wan DC, 2016a. Multi-resolution MPS method for free surface flows. *International Journal of Computational Methods*, **13**(4), 1641018-1-1641018- 17.
DOI: 10.1142/S0219876216410188

Tang ZY, Zhang YL, Wan DC, 2016b. Numerical simulation of 3-D free surface flows by overlapping MPS. *Journal of Hydrodynamics*, **28**(2), 306-312.
DOI: 10.1016/S1001-6058(16)60632-7

Walhorn E, Kölke A, Hübner B, Dinkler D, 2005. Fluid-structure coupling within a monolithic model involving free surface flows. *Computers & Structures*, **83**(25-26), 2100-2111.
DOI: 10.1016/j.compstruc.2005.03.010

Zhang YL, Tang ZY, Wan DC, 2016. Numerical investigations of waves interacting with free rolling body by modified MPS method. *International Journal of Computational Methods*, **13**(4), 1641013-1-1641013-14.
DOI: 10.1142/S0219876216410139

Zhang YL, Wan DC, 2017. Numerical study of interactions between waves and free rolling body by IMPS method. *Computers & Fluids*, **155**, 124-133.
DOI: 10.1016/j.compfluid.2017.03.019

Zhang YX, Wan DC, 2011. Application of MPS in 3D dam breaking flows. *Sci. Sin. Phys. Mech. Astron*., **41**, 140-154.
DOI: 10.1360/132010-1195

Zhang YX, Wan DC, 2012. Numerical simulation of liquid sloshing in low-filling tank by MPS. *Chinese Journal of Hydrodynamics*, **27**(1), 100-107. (in Chinese)
DOI: 10.3969/j.issn1000-4874.2012.01.015

Zhang YX, Wan DC, Hino T, 2014. Comparative study of MPS method and level-set method for sloshing flows. *Journal of hydrodynamics*, **26**(4), 577-585.
DOI: 10.1016/S1001-6058(14)60065-2